

Thermodynamics of a Modified Fermi-Hubbard Model

Moorad Alexanian

*Department of Physics and Physical Oceanography
University of North Carolina Wilmington, Wilmington, NC 28403-5606*

E-mail: alexanian@uncw.edu

(Received: July 20, 2024; Revised: August 25, 2024; Accepted: August 30, 2024)

Abstract. A recently introduced recurrence-relation ansatz applied to the Fermi-Hubbard model gives rise to a soluble model and here is used to calculate several thermodynamic observables. The constraint of unit density per site, $\rho = 1$, is applied and some of the results are compared to cases where the constraint is not imposed. The modified model exhibits a continuous phase transition (second order) reminiscent of the integer quantum Hall resistance and a ground state, first-order phase transition.

Keywords: Fermi-Hubbard model, recurrence-relation ansatz, modified Fermi-Hubbard model, grand canonical ensemble, thermodynamic observables, universality, phase transition

DOI:10.54503/18291171-2024.17.2-34

1. Introduction

The Fermi-Hubbard model has become the basis for much of what we know about superfluidity in periodic systems, quantum magnetism, and strongly correlated fermion physics on lattices in general [1]. We consider a recently introduced recurrence-relation ansatz for the hopping part of the Fermi-Hubbard model giving rise to an exactly soluble [2]. We use the latter model in this work to calculate several thermodynamic observables and consider possible universality viz-à-viz the number N of distinguishable microstates [3].

This paper is structured as follows. In Sec. 2, we present the Fermi-Hubbard model on an infinite, one-dimensional lattice. In Sec. 3, we introduce a recurrence-relation ansatz for the external degree of freedom associated with the nearest neighbor of the j -th lattice site. In Sec. 4, the grand canonical partition function is determined. In Sec. 5, the density, number of on-site pairs, compressibility, etc. are calculated. In Sec. 6, the total energy, specific heat, and entropy are determined. Finally, Sec. 8 summarizes our results.

2. Fermi-Hubbard model

The SU(N) Fermi-Hubbard model is given by [4, 5]

$$\hat{H} = -t \sum_{\langle i,j \rangle, \sigma} (\hat{c}_{i\sigma}^\dagger \hat{c}_{j\sigma} + \hat{c}_{j\sigma}^\dagger \hat{c}_{i\sigma}) + \frac{U}{2} \sum_{i, \sigma \neq \tau} \hat{n}_{i\sigma} \hat{n}_{i\tau} - \mu \sum_{i, \sigma} \hat{n}_{i\sigma}, \quad (1)$$

where $\hat{c}_{i\sigma}^\dagger$ and $\hat{c}_{i\sigma}$ represent the fermionic creation and annihilation operators at site i with spin σ is the number operator, $\langle i, j \rangle$ denotes adjacent sites on a rectangular lattice, t is the hopping amplitude, U is the on-site interaction strength, and μ denotes the chemical potential. Representing the Fermi-Hubbard Hamiltonian on a quantum computer requires a fermionic encoding. The well-known Jordan-Wigner transform is used, under which each

fermionic mode maps to one qubit, interpreted as lying on a 1D line [4]. Since we are interested in comparing our numerical results to those where universality in the number of distinguishable microstates N is considered, we are assuming that all sites have the same chemical potential μ [3].

3. Ansatz

Consider the following recurrence-relation ansatz [2] for the term associated with the hopping term of the i -th lattice in (1)

$$\hat{c}_{i+1\sigma} = \hat{c}_{i\sigma} - \hat{c}_{i-1\sigma}. \quad (2)$$

and so

$$\sum_{i,\sigma} \left[\hat{c}_{i\sigma}^\dagger \hat{c}_{i+1\sigma} + \hat{c}_{i+1\sigma}^\dagger \hat{c}_{i\sigma} + \hat{c}_{i\sigma}^\dagger \hat{c}_{i-1\sigma} + \hat{c}_{i-1\sigma}^\dagger \hat{c}_{i\sigma} \right] = 2 \sum_{i,\sigma} \hat{c}_{i\sigma}^\dagger \hat{c}_{i\sigma} = 2 \sum_i \hat{n}_i, \quad (3)$$

$$\hat{n}_i = \sum_\sigma \hat{n}_{i\sigma}.$$

where It is clear from (3) that we are considering a truly infinite one-dimensional lattice rather than an open-ended infinite chain.

More generally on may consider the ansatz that applies to both the infinite lattice, as well as, the open-ended infinite chain, viz.,

$$\hat{c}_{i+1\sigma}^\dagger = (\alpha + i\beta) \hat{c}_{i\sigma}^\dagger, \quad (4)$$

with α and β real. Therefore,

$$\sum_{i=-\infty,\sigma}^{\infty} \left[\hat{c}_{i\sigma}^\dagger \hat{c}_{i+1\sigma} + \hat{c}_{i+1\sigma}^\dagger \hat{c}_{i\sigma} + \hat{c}_{i\sigma}^\dagger \hat{c}_{i-1\sigma} + \hat{c}_{i-1\sigma}^\dagger \hat{c}_{i\sigma} \right] = 4\alpha \sum_{i=-\infty,\sigma}^{\infty} \hat{c}_{i\sigma}^\dagger \hat{c}_{i\sigma} = 4\alpha \sum_{i=-\infty}^{\infty} \hat{n}_i \quad (5)$$

and

$$\sum_{i=1,\sigma}^{\infty} \left[\hat{c}_{i\sigma}^\dagger \hat{c}_{i+1\sigma} + \hat{c}_{i+1\sigma}^\dagger \hat{c}_{i\sigma} \right] = 2\alpha \sum_{i=1,\sigma}^{\infty} \hat{c}_{i\sigma}^\dagger \hat{c}_{i\sigma} = 2\alpha \sum_{i=1}^{\infty} \hat{n}_i. \quad (6)$$

The left-hand-side of (4) obeys the same anticommutation relations as the right-hand-side of (4) provided $\alpha^2 + \beta^2 = 1$. In what follows, we will consider the infinite lattice with ansatz (2), that is, $\alpha = 1/2$ in (5), which is the same as for the open-ended infinite chain but with $\alpha = 1$ in (6).

The Fermi-Hubbard model (1) is reduced to

$$\begin{aligned} \hat{H} &= -2t \sum_i \hat{n}_i + \frac{U}{2} \sum_{i,\sigma \neq \tau} \hat{n}_{i\sigma} \hat{n}_{i\tau} - \mu \sum_{i,\sigma} \hat{n}_{i\sigma}, \\ &= -2t \sum_i \hat{n}_i + \frac{U}{2} \sum_i \hat{n}_i^2 - \frac{U}{2} \sum_i \hat{n}_i - \mu \sum_i \hat{n}_i, \end{aligned} \quad (7)$$

$$\hat{n}_{i\sigma}^2 = \hat{n}_{i\sigma}$$

since with energy eigenvalues

$$E_i = -2tn_i + \frac{U}{2}n_i^2 - \frac{U}{2}n_i - \mu n_i. \quad (8)$$

4. Grand canonical partition function

The grand canonical partition function is the following product over the differing lattices sites

$$\mathcal{Z} = \prod_{i,\sigma} e^{-\beta E_i}, \quad (9)$$

where $\beta = 1/k_B T$ and we consider N_s lattice sites with each containing up to N distinguishable microstates σ , viz., and $\sum_i n_i = N$ so $\sum_i \langle \hat{n}_i \rangle = N$. One obtains, with the aid of (8),

$$\mathcal{Z} = \prod_i \sum_{n=0}^N \frac{N!}{n!(N-n)!} e^{[(2t/U+1/2+\mu/U)n-n^2/2]U/(k_B T)} = \prod_i \sum_{n=0}^N \frac{N!}{n!(N-n)!} e^{(\tilde{\mu}n-n^2/2)/\tilde{T}}, \quad (10)$$

where the renormalized chemical potential $\tilde{\mu}_i$ and the scaled temperature \tilde{T} are given by [2]

$$\tilde{\mu} = 2t/U + 1/2 + \mu/U \quad \text{and} \quad \tilde{T} = k_B T/U \quad (11)$$

and the binomial coefficient $\frac{N!}{n!(N-n)!}$ represents the distribution of n , $n = 0 \dots N$, distinguishable microstates in the i -th, $i = 1 \dots N$, distinguishable lattice sites with all parameters expressed in units of U . Accordingly, there are only the variables N , $\tilde{\mu}$ for each lattice site i , and \tilde{T} .

It is important to remark that a given value of the renormalized chemical potential $\tilde{\mu}$ does not determine the individual values of either t/U or μ/U . It is clear that our modified Fermi-Hubbard model reduces to the original Fermi-Hubbard model for $t = 0$. It may be that the results from the modified Fermi-Hubbard model for $t > 0$ and $\mu \gg t$ reproduce those of the original Fermi-Hubbard model. In what follows, we calculate various thermodynamic observables for the modified Fermi-Hubbard model given by the grand partition function (10).

5. Density ρ , number of on-site pairs D , compressibility κ , dependence on chemical potential μ/t , and $dD/d\rho$ on ρ

The average number $\langle \hat{n} \rangle$ of microstates in a lattice site with chemical potential $\tilde{\mu}$ and temperature \tilde{T} is given by

$$\rho \equiv \langle \hat{n} \rangle = k_B T \frac{\ln \mathcal{Z}}{\partial \mu} = \frac{\sum_{n=0}^N \frac{N!}{n!(N-n)!} n e^{(\tilde{\mu}n-n^2/2)/\tilde{T}}}{\sum_{n=0}^N \frac{N!}{n!(N-n)!} e^{(\tilde{\mu}n-n^2/2)/\tilde{T}}}. \quad (12)$$

Fig.1(a) shows the density dependence on chemical potential $(\mu - \mu_0)/t$ for $N = 2, 3, 4$, $U/t = 8$ at $T/t = 0.5$ and where μ_0 is defined by $\rho(\mu_0) = 1$. Note that the universality in N holds for $-5 < (\mu - \mu_0)/t < 10$, which is a larger region than that considered in [3], viz., $-5 < (\mu - \mu_0)/t < 5$. The existence of the phase transition is evident for large values of $(\mu - \mu_0)/t$ via the corresponding steps as indicated previously [2].

The number of on-site pairs per site is

$$D \equiv \frac{1}{N_s} \sum_i \left[\frac{1}{2} \sum_{\alpha \neq \tau} \langle \hat{n}_{i\alpha} \hat{n}_{i\tau} \rangle \right] = \frac{1}{2N_s} \sum_i [\langle \hat{n}_i^2 \rangle - \langle \hat{n}_i \rangle^2] = \frac{1}{2} (\langle \hat{n}^2 \rangle - \langle \hat{n} \rangle^2), \quad (13)$$

where the last equality follows since all the lattice sites are identical, that is, have the same chemical potential μ . The isothermal compressibility is defined by

$$\kappa_T \equiv \left(\frac{\partial \langle \hat{n} \rangle}{\partial \mu} \right)_T = T^{-1} (\langle \hat{n}^2 \rangle - \langle \hat{n} \rangle^2), \quad (14)$$

where N_s is the number of sites and $\hat{n}_i^2 = \hat{n}_i$ for fermions. Fig.1(b) is a plot of the number of on-site pairs D versus $(\mu - \mu_0)/t$ for $N = 2, 3, 4$, $U/t = 8$ at $T/t = 0.5$ and where μ_0 is defined by $\rho(\mu_0) = 1$. Note again where universality, that is, independence of N , occurs in a larger region as in Fig.1(a) than that obtained in [3]. The asymptotic value is given by $N(N - 1)/2$. Figs.1(c, d) are plots of the isothermal compressibility κ and $dD/d\rho$, for the same values as those in Figs.1(a, b). The universality in the isothermal compressibility κ is the same as that in Figs.1(a, b) and the range where κ is periodic increasing with increasing values of N . However, universality in $dD/d\rho$ as shown in Fig.1(d) is limited to $\rho < 1$ with step function behavior.

The asymptotes for ρ and D are reached for $(\mu - \mu_0)/t \approx 5(N = 2)$, $15(N = 3)$, $25(N = 4)$ as seen in Figs.1(a, b). Whereas the stepwise asymptotic behavior in Fig.1(d) represents actually a continuous phase transition (second order), which disappears at higher temperatures [2]. The stepwise behavior is reminiscent of the integer quantum Hall resistance [6, 7].

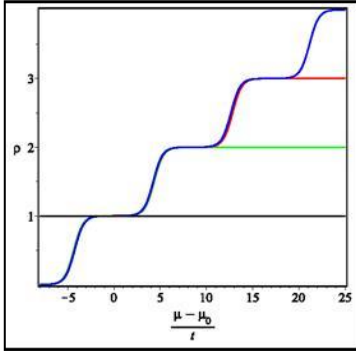


Fig. 1a. Density ρ dependence on chemical potential, where $\rho(\mu_0) = 1$, $N=2$ (green), 3 (red), 4 (blue). $U/t = 8$ and $T/t = 0.5$.

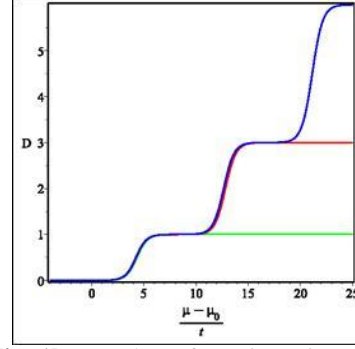


Fig. 1b. Number of on-site pairs dependence D on chemical potential, where $\rho(\mu_0) = 1$, $N=2$ (green), 3 (red), 4 (blue). $U/t = 8$ and $T/t = 0.5$.

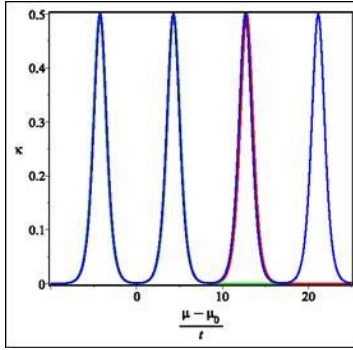


Fig. 1c. Compressibility κ dependence on chemical potential, where $\rho(\mu_0) = 1$, $N=2$ (green), 3 (red), 4 (blue). $U/t = 8$ and $T/t = 0.5$.

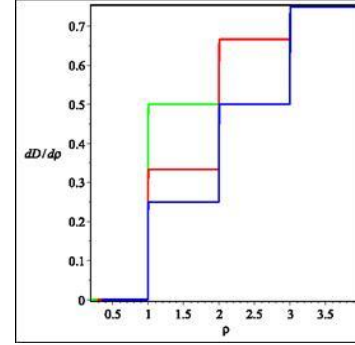


Fig. 1d. Derivative of the number of on-site pairs D with respect to the density $dD/d\rho$ as a function of density, where $\rho(\mu_0) = 1$, $N=2$ (green), 3 (red), 4 (blue). $U/t = 8$ and $T/t = 0.5$.

Fig.2(a-d) show the behavior of the number of on-site pairs D as a function of temperature T/t . Each panel compares D for $N = 2, 3, 4$ for fixed values of U/t and $\rho = 1$. Universality occurs for large values of U/t when our modified model approaches the results of the Fermi-Hubbard model. We were not able to include the case for $N = 6$, which gives rise to a fifth order polynomial and no closed-form solutions exist for general fifth or higher order polynomial equations. In Fig.3(a-d), each panel compares D for $U/t = 4, 8, 12, 40$ for fixed $N = 2, 3, 4$. Universality seems to occur for small values of T/t since one has that as $T \rightarrow \infty$, $D \rightarrow 1/4, 1/3, 3/8$ for $N = 2, 3, 4$, respectively.

6. Total energy, specific heat, entropy

The energy E , the entropy S , and the specific heat C follow from the grand canonical partition function \mathcal{Z}

$$E = T^2 \frac{\partial \ln \mathcal{Z}}{\partial T} + \mu T \frac{\partial \ln \mathcal{Z}}{\partial \mu}, \quad C = \frac{\partial E}{\partial T}, \quad \text{and} \quad S = \ln \mathcal{Z} + T \frac{\partial \ln \mathcal{Z}}{\partial T}, \quad (15)$$

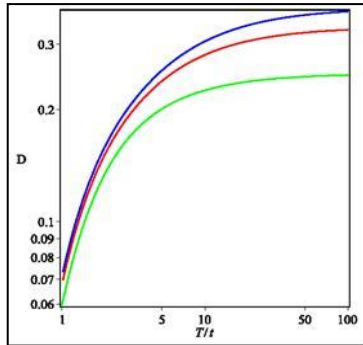


Fig. 2a. Number of on-site pairs D versus temperature for $N = 2$ (green), 3 (red), 4 (blue) for $U/t = 4$ and $\rho = 1$.

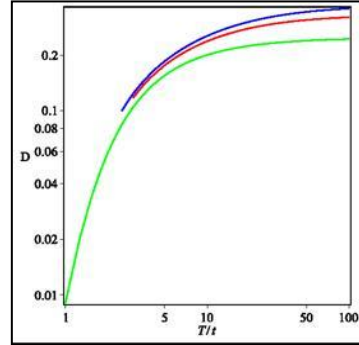


Fig. 2b. Same as Fig.2(a) but with $U/t = 8$.

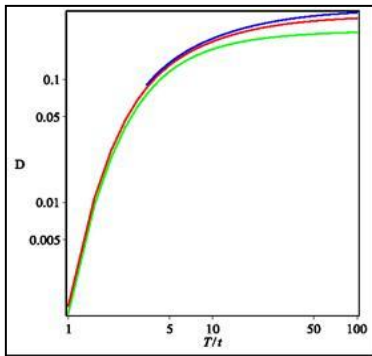


Fig. 2c. Same as Fig.2(a) but with $U/t = 12$.

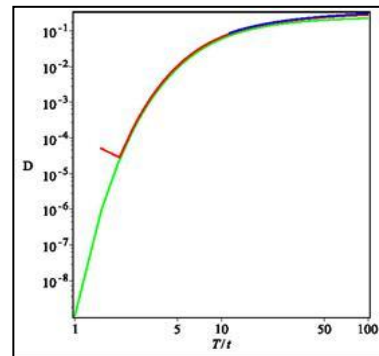


Fig. 2d. Same as Fig.2(a) but with $U/t = 40$.

where we have set $k_B = 1$. We shall consider, in evaluating these thermodynamic observables, the cases of lattices with $N = 2, 3, 4$ and equal chemical potentials μ .

Fig.4(a-d) shows the energy per site for different values of U/t . One has universality in a larger region than previously $0 \leq T/t < 5$. Actually, this behavior follows from the requirement that $\rho = 1$ since as $T \rightarrow 0$, $E \rightarrow K$ and the kinetic energy per site K is

$$K/t = -\frac{1}{N_s} \sum_{\langle i,j \rangle, \sigma} (\hat{c}_{i\sigma}^\dagger \hat{c}_{j\sigma} + \hat{c}_{j\sigma}^\dagger \hat{c}_{i\sigma}) = -2\rho, \quad (16)$$

with the aid of ansatz (3). The requirement that $\rho = 1$, gives rise to a value of -2 for the kinetic energy per site in the limit $T \rightarrow 0$, as indicated in Fig.4 for all values of U/t and N . In the limit $T \rightarrow \infty$, one has for the plots in Fig.4(a) the limits $-1(N=2)$, $-2/3(N=3)$, $-1/2(N=4)$. For Fig.4(b), $0(N=2)$, $2/3(N=3)$, $1(N=4)$. For Fig.4(c) $1(N=2)$, $2(N=3)$, $5/2(N=4)$. Finally, for Fig.4(d), $8(N=2)$, $34/3(N=3)$, $13(N=4)$.

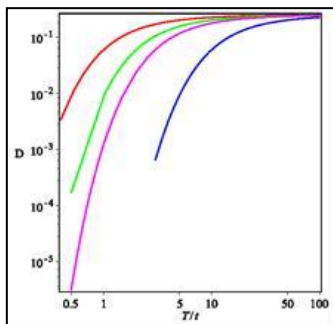


Fig. 3a. Number of on-site pairs D versus temperature for $U/t = 4$ (green), 8 (red), 12 (magenta), and 40 (blue) for $N=2$ with $\rho = 1$.

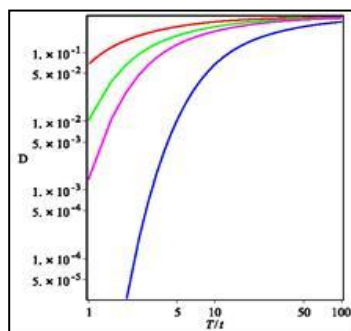


Fig. 3b. Same as Fig.3a but for $N=3$.

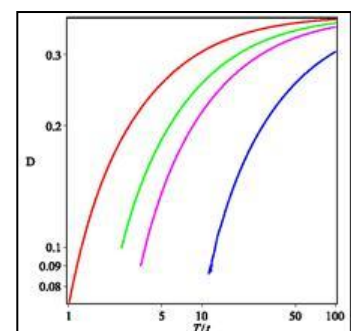


Fig. 3c Same as Fig.3a but for $N=4$.

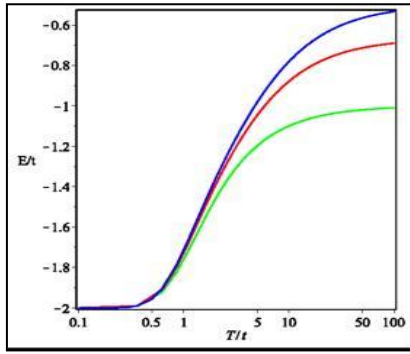


Fig. 4a. Energy per site E versus temperature T for $N = 2$ (green), 3 (red), 4 (blue) for $U/t = 4$ with $\rho = 1$.

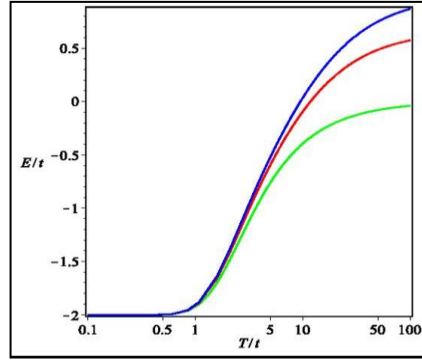


Fig. 4b. Same as Fig.4a but with $U/t = 8$.

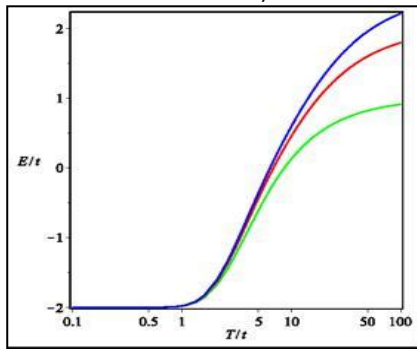


Fig. 4c. Same as Fig.4a but with $U/t = 12$.

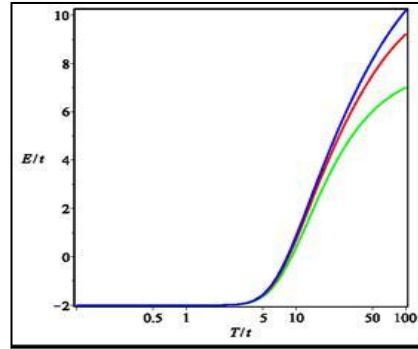


Fig. 4d. Same as Fig.4a but with $U/t = 40$.

The high and low temperature behaviors of the energy can be ascertained for the cases indicated in Fig.4, where the condition $\rho = 1$ has been imposed. However, when the total energy is expressed in terms of the renormalized $\tilde{\mu}$ and the scaled temperature \tilde{T} one obtains, when the restriction $\rho = 1$ is not imposed, that

$$\begin{aligned} E &\rightarrow \frac{1}{8}N(N+1)N_s & (T \rightarrow \infty), \\ E &\rightarrow \frac{1}{2}N^2N_s & (\tilde{\mu} \rightarrow \infty), \end{aligned} \quad (17)$$

depending only on N . The latter limit can be seen in Fig.10 of [2], where one has for $N = N_s = 6$, the limiting value of $E = 108$. The corresponding limit $T \rightarrow 0$ behavior will be discussed below, where the phase transition is made evident.

The specific heat is shown in Fig.5. Note that the location of the peaks are almost independent of N and increases with temperature as U/t increases. Our results do not seem to agree with those in [3]. In Fig.6 one has that the entropy increases with increasing N for given T/t . The behavior of the entropy at low and high temperatures for the case with $\rho = 1$, differs considerably from cases where the requirement $\rho = 1$ is not imposed. In the former case one has

$$\begin{aligned} S/N_s &= \ln N & \text{at } T = 0 \\ S/N_s &= N \ln N - (N-1) \ln(N-1) & \text{as } T \rightarrow \infty, \end{aligned} \quad (18)$$

as attested in Fig.6.

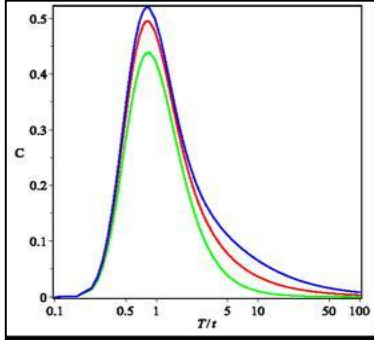


Fig. 5a. Specific heat versus temperature for $N = 2$ (green), 3 (red), 4 (blue) for $U/t = 4$ with $\rho = 1$.

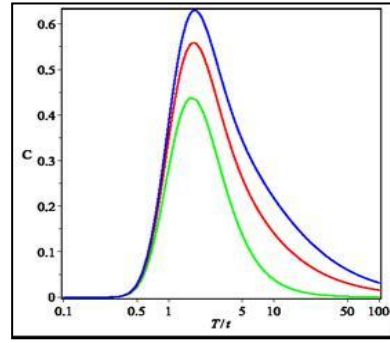


Fig. 5b. Same as Fig.5a but with $U/t = 8$.

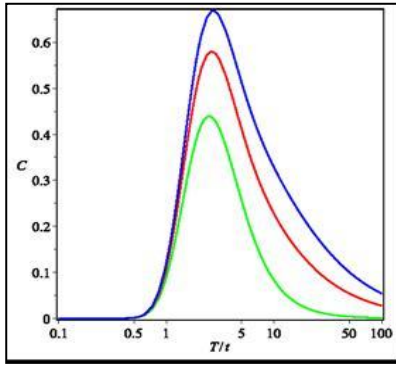


Fig. 5c. Same as Fig.5a but with $U/t = 12$.

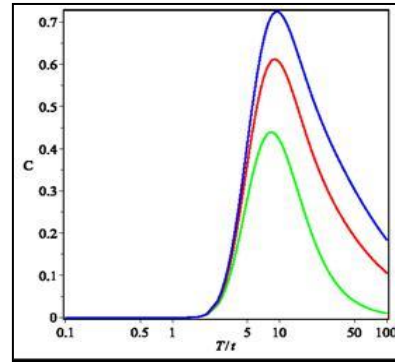


Fig. 5d. Same as Fig.5a but with $U/t = 40$.

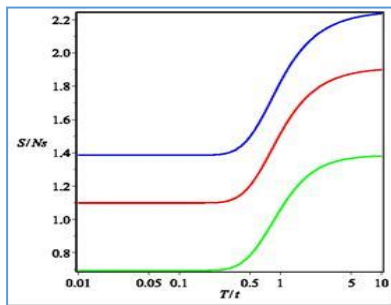


Fig. 6a. Entropy per site versus temperature for $N = 2$ (green), 3 (red), 4 (blue) for $U/t = 4$ with $\rho = 1$.

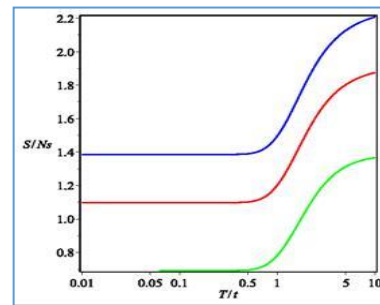


Fig. 6b. Same as Fig.6a but with $U/t = 8$.

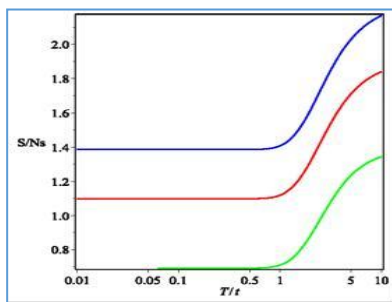


Fig. 6c. Same as Fig.6a but with $U/t = 12$.

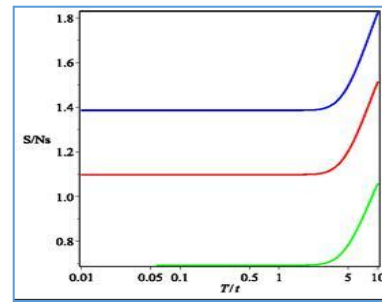


Fig. 6d. Same as Fig.6a but with $U/t = 40$.

In the general case where the condition $\rho = 1$ is not imposed, we obtain

$$S/N_s = \ln \left(\frac{4!}{\left(\frac{3}{4} + \frac{1}{8} \frac{\mu}{t}\right)! \left(\frac{13}{4} - \frac{1}{8} \frac{\mu}{t}\right)!} \right) \quad \text{at} \quad T = 0 \tag{19}$$

$$S/N_s = N \ln 2 \quad \text{as} \quad T \rightarrow \infty,$$

where N microstates in a given site have 2^N dimensions and so we can form N pairs of two-qubit entangled states each with a maximum entropy $\ln 2$ giving rise to a total entropy per site of $N \ln 2$. (see Fig.13 in [2], plot of total entropy with $N = N_s = 6$, which corresponds to our Fig.7(b) for the entropy per site S/N_s). The values for μ/t indicated in the caption of Fig.7(a) corresponds to the values of the renormalized chemical potential, $\tilde{\mu} = 0, 1, 2, 3, 4$, where the constraint $\rho = 1$ is not imposed on the results. The plot in Fig.7(c) is the zero-temperature, scaled energy per site versus N for $\tilde{\mu} = 6$, where the constraint $\rho = 1$ is not imposed on the results,

$$\begin{aligned} E/(UN_s) &= \frac{\tilde{\mu}^2}{2} & \tilde{\mu} \leq N \quad (\text{constant}) \\ &= \frac{N^2}{2} & \tilde{\mu} > N \quad (\text{steps}). \end{aligned} \quad (20)$$

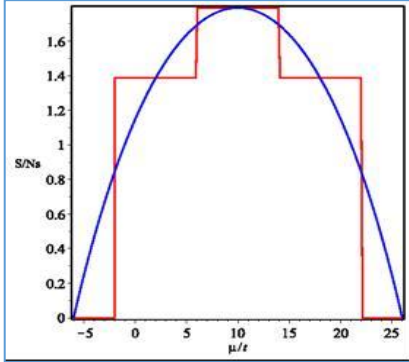


Fig. 7a. Zero temperature behavior of the entropy per site S/N_s (red) and $\ln(N!/[\tilde{\mu}!(N - \tilde{\mu})!])$ (blue) versus μ/t , where $\tilde{\mu} = 2t/U + 1/2 + \mu/U$. For $N = 4$ lattice sites all with the same chemical potential and $U/t = 8$, $S/N_s = 0$ for $\mu/t = -6, 26$, $S/N_s = \ln(4) = 1.38 \dots$ for $\mu/t = 2, 18$, $S/N_s = \ln(6) = 1.79 \dots$ for $\mu/t = 10$.

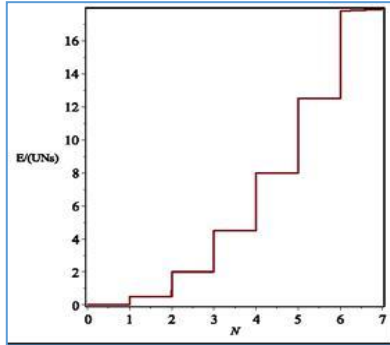


Fig. 7c. Zero temperature behavior of the energy per site $E/(UN_s)$ for $\tilde{\mu} = 6$ as a function of N . For $N \geq 6$ the energy is constant with value 18. The steps are for $N < 6$ corresponding to steps with height $N^2/2$.

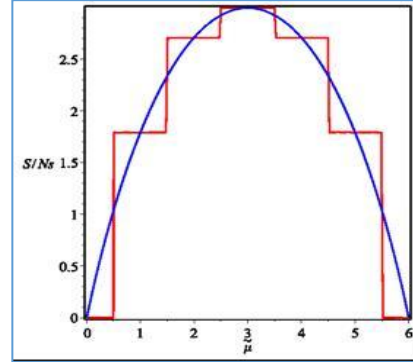


Fig. 7b. Zero temperature behavior of the entropy per site S/N_s (red) and $\ln(N!/[\mu!(N - \mu)!])$ (blue) versus renormalized $\tilde{\mu} = 2t/U + 1/2 + \mu/U$ for $N = 6$ lattice sites all with the same chemical potential $\tilde{\mu}$. $S/N_s = 0$ for $0 < \tilde{\mu} < 1/2$ and $11/2 < \tilde{\mu}$, $S/N_s = \ln(6) = 1.79 \dots$ for $1/2 < \tilde{\mu} < 3/2$ and $9/2 < \tilde{\mu} < 11/2$, $S/N_s = \ln(15) = 2.70 \dots$ for $3/2 < \tilde{\mu} < 5/2$ and $7/2 < \tilde{\mu} < 9/2$, $S/N_s = \ln(20) = 2.99 \dots$ for $5/2 < \tilde{\mu} < 7/2$.

Note that there is energy saturation for given renormalized chemical potential.

7. Conclusions

We consider further an exactly soluble, modified Fermi-Hubbard model in order to calculate thermodynamic observables and compare them to recently obtained numerical results that place the density constraint $\rho = 1$. It is not clear why the latter constraint; it may simplify the numerical

computations. The modified model exhibits a continuous phase transition (second order) reminiscent of the integer quantum Hall resistance and a ground state, first-order phase transition. In the absence of said constraint, the high temperature behavior of the entropy per site shows maximal entanglement $N \ln 2$, where N is the number of microstates in a given lattice site.

References

- [1] N. Gemelke, *Physics* **9** (2016) 44.
- [2] M. Alexanian, *Arm. J. Phys.* **17** (2024) 1.
- [3] E. Ibarra-García-Padilla, S. Dasgupta, H.-T. Wei, S. Taie, Y. Takahashi, R.T. Scalettar, K.R.A. Hazzard, *Phys. Rev. A* **104** (2021) 043316
- [4] S. Stanistic, J.L. Bosse, F.M. Gambetta, R.A. Santos, W Mruczkiewicz, T.E. O'Brien, E. Ostby, A. Montanaro,, *Nature Commun.* **13** (2022) 5743.
- [5] G. Pasqualetti, O. Bettermann, N. Darkwah Oppong, E. Ibarra-García-Padilla, S. Dasgupta, R. T. Scalettar, K. R. A. Hazzard, I. Bloch, and S. Fölling, *Phys. Rev. Lett.* **132** (2024) 083401.
- [6] K. von Klitzing, G. Dorda, M. Pepper, *Phys. Rev. Lett.* **45** (1980) 494.
- [7] K. von Klitzing, *Rev. Mod. Phys.* **58** (1986) 519.